Electronic Supplementary Information (ESI)

Colloidal $BaZrS_3$ Chalcogenide Perovskite Nanocrystals for Thin Film Device Fabrication

Vikash Kumar Ravi,[a] Seong Hoon Yu,[b] Parikshit Kumar Rajput,[a] Chandrani Nayak,[c] Dibyendu Bhattacharyya,[c] Dae Sung Chung,*[b] Angshuman Nag*[a]

[a]Department of Chemistry Indian Institute of Science Education and Research (IISER), Pune-411008, India.

[b]Department of Chemical Engineering, Pohang University of Science and Technology (POSTECH), Pohang 37673, Republic of Korea.

[c]Atomic & Molecular Physics Division, Bhabha Atomic Research Centre, Mumbai- 400085, India.

*Corresponding authors' e-mails: AN: angshuman@iiserpune.ac.in

DSC: dchung@postech.ac.kr

Experimental Section:

Chemicals: Barium sulfide (BaS, 99.9%, Sigma-Aldrich), sulfur (S, 99.998%, Sigma-Aldrich), zirconium powder (99%, Nanoshel), iodine (I_2, 99.9%, Rankem) oleylamine (OAm, technical grade 70%, Sigma-Aldrich), zirconium tetrachloride ($ZrCl_4$, 99.99%, Sigma-Aldrich), barium chloride ($BaCl_2$, 99.99%, Sigma Aldrich), carbon disulfide (CS_2, >99%, Sigma Aldrich), methyl acetate (anhydrous, 99.5%, Sigma-Aldrich), hexylamine (99%,, Sigma-Aldrich), octanoic acid (>99%, Sigma-Aldrich), thioglycolic acid(≥98%, Sigma-Aldrich), tetrabutylammonium bromide (≥98%, Sigma-Aldrich), N-methyl-2-pyrrolidinone (90.7%, Sigma-Aldrich), chloroform ($CHCl_3$, ≥99 % D, Sigma-Aldrich), methylene blue (Sigma-Aldrich).

Solid state synthesis of $BaZrS_3$ nanocrystals (NCs) powder:

Solid state synthesis of $BaZrS_3$ NCs powder is done by following modified method of Niu et al.[1] Stoichiometric amount of BaS, Zr and S powders (BaS = 3 mmol, Zr = 3 mmol, and S = 6 mmol), and catalytic amount of iodine (25 mg) are taken inside a quartz tube. The quartz tube has length 20 cm, outer diameter of 20 mm and inner diameter of 18 mm. The tube containing the chemicals are then put under high vacuum of 5×10^{-6} mbar. Then the tube is sealed using oxy-acetylene torch and put inside a tubular furnace. The reaction is then carried out at 600 °C for 60 hours with heating rate of 1 °C/min and cooling rate of 0.5 °C/min. After the completion of reaction, the tube is taken out of the furnace and it is broken to take out the black-brown powder as shown in Figure S1. It is then further grinded to finer powder. These grinded powders are used for all characterization and surface modification. After the completion of the reaction, we observe purple colored depositions in the walls of sealed quartz tube, probably because of the deposition of the I_2 vapor. Note that, we could not detect the presence of iodine in the product $BaZrS_3$ nanocrystal.

Surface modification to form colloidal $BaZrS_3$ NCs:

To achieve colloidal dispersion of $BaZrS_3$ NCs, first we mix $BaZrS_3$ NCs powder with N-methyl-2-pyrrolidinone and then stirred the mixture at 120 °C for 6 hours to make it completely dispersible. It yields dark brownish dispersion which was then passed from 0.22 μm syringe filter without any aggregation to obtain stable dispersion of $BaZrS_3$ NCs in N-methyl-2-pyrrolidinone. Further to obtain colloidal dispersion of $BaZrS_3$ NCs in low boiling solvent like $CHCl_3$, we did a second round of surface modification by taking a mixture of $BaZrS_3$ NCs (400 mg) in N-methyl-2-pyrrolidinone 300 μL along with 100 μL OAm and

heated it at 160 °C till the majority of solvent evaporates and it dries to form a thick paste. Then the dried paste is dispersed into $CHCl_3$ and passed through the syringe filter to obtain stable colloidal dispersion of $BaZrS_3$ in $CHCl_3$.

Our unsuccessful attempts of direct colloidal synthesis of $BaZrS_3$ NCs:

Traditional synthesis for NCs like CdS, PbS or even recently developed lead halide perovskites relies on the popular "hot injection method" to obtain colloidal high quality NCs. It involves complexation of precursors in a suitable reaction medium with a suitable ligand followed by "hot injection" of remaining precursor at higher temperature. However, for the synthesis of colloidal $BaZrS_3$ NCs, this knowledge is still lacking. We attempted to synthesize colloidal $BaZrS_3$ NCs by choosing our precursor as $ZrCl_4$, $BaCl_2$ and CS_2. We got motivated by the report of ZrS_2 nanodiscs synthesis as reported by Jang et al.[2] Briefly, $ZrCl_4$ (1.5 mmol) and $BaCl_2$ (1.5 mmol) were taken in 3 neck round bottom flask with OAm (5.0 g). The reaction mixture was alternately put under vacuum and then purged with N_2 for 30 min (repeated 2 times). The reaction mixture temperature was then raised to 300 °C and 0.3 mL CS_2 (5 mmol) was injected. The reaction was allowed to go for 1 hour and then stopped and cooled down to room temperature. The product obtained was washed using (1:2 V/V) mixture of hexane: 1-butanol. However, this approach didn't yield any positive result. The PXRD pattern recorded on the obtained product shows presence of unwanted compounds like BaS and ZrS_2. We attribute this to the competition between Ba and Zr for the ease in forming their respective sulfides compared to $BaZrS_3$ perovskites. We do hope that a proper selection of reactive precursor, optimization of ligands and reaction temperature would result in colloidal synthesis of $BaZrS_3$ NCs in the near future. One of the plausible sulfur precursors can be dodecanethiol (DDT). DDT is known to slowly decompose to release hydrogen sulfide (H_2S) at temperature of ~ 240 °C for long hours (~10 hours) which would then suppress the nucleation burst giving impurity products.

Our attempts for $BaZrS_3$ NCs surface modification to improve charge transport:

We have attempted two strategies to improve the electronic connectivity between NCs: (i) treating the film to remove OAm, and (ii) searching for shorter ligands for obtaining colloidal dispersion of $BaZrS_3$ NCs.

Removal or partial removal of OAm from the NC film by both annealing at higher temperatures and treating with methyl acetate, resulted into the formation of craters or cracks

in the film. This issue restricts the observed carrier mobility. We strongly believe that the carrier mobility values will increase significantly, if we can solve this issue in future.

Another approach that we tried is, by exploring different shorter ligands for obtaining stable dispersion of $BaZrS_3$ NCs. We have tried different ligands like hexylamine, thioglycolic acid, octanoic acid, and tetrabutylammonium bromide as ligand for $BaZrS_3$ NCs. In the case of hexylamine and octanoic acid, we did not obtain any colloidal dispersion of $BaZrS_3$ NCs. Thioglycolic acid (or other thiols) leads to the degradation of $BaZrS_3$ chalcogenide to white product. For tetrabutylammonium bromide ligand case, we do obtain colloidal dispersion but the NCs precipitate within 10-15 minutes. The binding of these ammonium halides are reported for metal chalcogenide NCs like PbS.[3]

Note that the $BaZrS_3$ NCs are pretty big in size (40-60 nm). The bigger size reduces colloidal stability, unless we find a suitable ligand. On the other hand, the big size of NCs reduces surface states and grain boundaries, therefore, improving the charge transport of NCs films.

Thin film preparation of $BaZrS_3$ NCs:

$BaZrS_3$ NCs dispersion in $CHCl_3$ (concentration of 10 mg/mL) is prepared by dispersing thick paste of surface modified $BaZrS_3$ NCs in $CHCl_3$ and stirring it for 3 hours at 50 °C to get a homogenous dispersion. To form $BaZrS_3$ NCs film, the dispersion is passed through the 0.2 μm filter without clogging, and spin coated for 30 s at 2000 rpm.

Characterization:

Powder X-ray diffraction (PXRD) patterns are recorded on Bruker D8 X-ray diffractometer with Cu Kα radiation of 1.54 Å**.** UV-visible-near infrared (NIR) diffused reflectance spectra of $BaZrS_3$ NCs powder are recorded using Shimadzu UV-3600 plus UV-VIS-NIR spectrophotometer. The reflectance data are converted to absorbance data using Kubelka-Munk transformation. The UV-visible absorption spectra of colloidal dispersion are recorded using Cary series UV-visible spectrophotometer. Steady state photoluminescence (PL) measurements are carried out using FLS 980 (Edinburgh Instruments). Transmission electron microscopy (TEM) images and high resolution TEM (HRTEM) images are captured by using a UHR FEG-TEM, JEOL JEM 2200FS field emission transmission electron microscope operated at 200 kV. TEM sample for $BaZrS_3$ NCs powder is prepared by taking ~ 0.5 mg of sample in n-butanol (~ 1 mL) and then drop casted on carbon coated Cu TEM grid, while colloidal $BaZrS_3$ NCs are drop casted directly on the TEM grid. Light intensity is measured using HTC Instrument LX-101A Light Meter Luxmeter. Surface morphology and thickness

of the films are determined using scanning electron microscopy (SEM) (Hitachi, SU8320) and atomic force microscopy (AFM) (Park systems, XE-150) respectively. The capacitance value of the dielectric layers is measured using Hewlett Packard 4284A LCR meter at 1 kHz. The electrical properties of devices are measured by Keithley 4200A-SCS in N_2-filled glove box.

Temperature dependent Extended X-ray absorption fine structure (EXAFS) measurement of $BaZrS_3$ NCs powder:

X-ray Absorption Spectroscopy **(**XAS) measurements of $BaZrS_3$ sample at different temperatures have been carried out at Zr K edge in transmission mode at the Scanning EXAFS Beamline (BL-09) at the Indus-2 Synchrotron Source (2.5 GeV, 200 mA) at the Raja Ramanna Centre for Advanced Technology (RRCAT), Indore, India.[4, 5] The beamline uses a double crystal monochromator (DCM) which works in the photon energy range of 4-25 KeV with a resolution of 10^4 at 10 KeV. A 1.5 m horizontal pre-mirror with meridional cylindrical curvature is used prior to the DCM for collimation of the beam and higher harmonic rejection. The second crystal of the DCM is a sagittal cylinder with radius of curvature in the range 1.28-12.91 meters which provides horizontal focusing to the beam while another Rh/Pt coated bendable post mirror facing down is used for vertical focusing of the beam at the sample position. For measurements in the transmission mode, the sample is placed between two ionization chamber detectors. The first ionization chamber measures the incident flux (I_0) and the second ionization chamber measures the transmitted intensity (I_T). From these intensities the absorbance of the sample (μ) is estimated as a function of energy as:

$$I_T = I_0 e^{-\mu x} \tag{1}$$

where, x is the thickness of the absorber.

For low temperature measurements the sample has been loaded in a closed cycle cryostat with kapton windows for X-ray transmission. For high temperature measurement the sample has been loaded in a stainless-steel cell with Be windows for X-ray transmission. The sample is mounted on a SS block in the cell which can be heated with two cartridge heaters. In this cell the temperature of the sample can go upto 400 °C (673 K). A thermocouple has been introduced in the cell from the top flange and is fixed at the sample holder touching the sample to record the exact temperature of the sample. The sample has been heated to high temperature in Ar atmosphere.

The EXAFS spectra have been extracted using the standard procedure.[6,7,8] In order to take care of the EXAFS oscillations in the absorption spectra, the energy dependent absorption coefficient $\mu(E)$ has been converted to absorption function $\chi(E)$ defined as follows:

$$\chi(E) = \frac{\mu(E) - \mu_0(E)}{\Delta\mu_0(E_0)} \qquad (2)$$

where E_0 absorption edge energy, $\mu_0(E_0)$ is the bare atom background and $\Delta\mu_0(E_0)$ is the step in the $\mu(E)$ value at the absorption edge. After converting the energy scale to the photoelectron wave number scale (k) as defined by,

$$k = \sqrt{\frac{2m(E - E_0)}{\mathrm{h}^2}} \qquad (3)$$

the energy dependent absorption coefficient $\chi(E)$ has been converted to the wave number dependent absorption coefficient $\chi(k)$, where m is the electron mass. Finally, $\chi(k)$ is weighted by k^2 to amplify the oscillation at high k and the functions $\chi(k)\,k^2$ are Fourier transformed in r space to generate the $\chi(r)$ versus r (or FT-EXAFS) spectra in terms of the real distances from the centre of the absorbing atom. The k range used for Fourier transform is 2-12 Å^{-1}. It should be mentioned here that a set of EXAFS data analysis program available within the IFEFFIT software package[9] have been used for reduction and fitting of the experimental EXAFS data. This includes data reduction and Fourier transform to derive the $\chi(r)$ versus r plots from the absorption spectra, generation of the theoretical EXAFS spectra starting from an assumed crystallographic structure and finally fitting of the experimental $\chi(r)$ versus r data with the theoretical ones using the FEFF 6.0 code.

Aqueous stability and photocatalytic activity of $BaZrS_3$ NCs powder:

As prepared $BaZrS_3$ NCs powder is studied as a photocatalyst for the degradation of methylene blue dye in water, under sunlight irradiation (~70 mW /cm^2). 100 ppm of methylene blue is prepared by dissolving 5 mg methylene blue in 50 mL Milli-Q water. The methylene blue solution is stirred in dark along with 20 mg $BaZrS_3$ NCs powder for 1 hour. This stirring promotes the chance for adsorption of dye on $BaZrS_3$ NCs powder. The degradation of methylene blue gets almost completed (ca. ~98 %) upon continuous irradiation of sun light over a period of 50 minutes. The photocatalytic dye degradation is repeated for multiple cycles, to test aqueous stability of $BaZrS_3$ NCs powder. The same

$BaZrS_3$ NCs is reused for all the cycles, along with addition of fresh methylene blue for each cycle.

Calculation of excitonic Bohr radius of $BaZrS_3$:

The excitonic Bohr radius, a_{exc} can be calculated using the formula:

$$a_{exc} = \frac{\varepsilon_r}{\mu} \times a_H \times m_0$$

where: ε_r is effective dielectric constant

μ is effective mass of exciton

a_H is Bohr radius of hydrogen (0.0529 nm)

m_0 is electron rest mass

For $BaZrS_3$ electron and hole mass[10]: $m_e = 0.30\ m_0$ and $m_h = 0.46\ m_0$

$$\mu = \frac{m_e \times m_h}{m_e + m_h} = 0.18\ m_0$$

For $BaZrS_3$, dielectric constant[11], $\varepsilon_r = 9.6$

Putting these values:

$$a_{exc} = 2.8\ nm$$

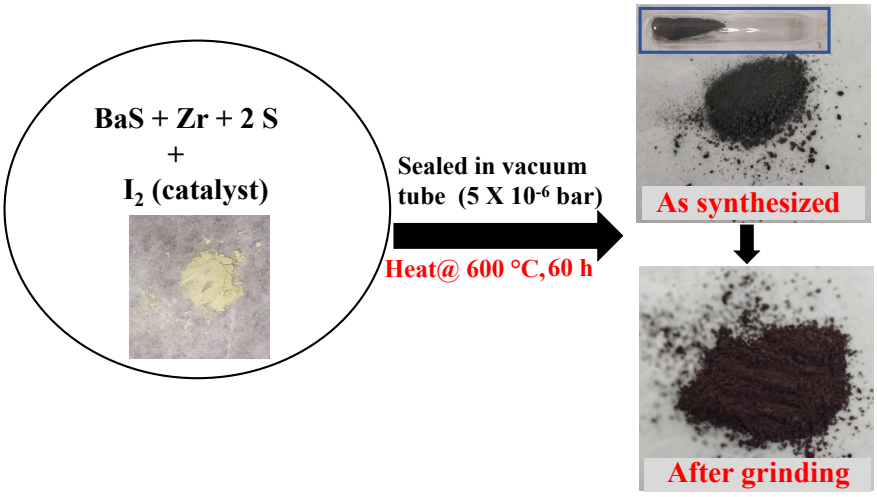

Figure S1: Schematic showing solid state synthesis of $BaZrS_3$ NCs powder.

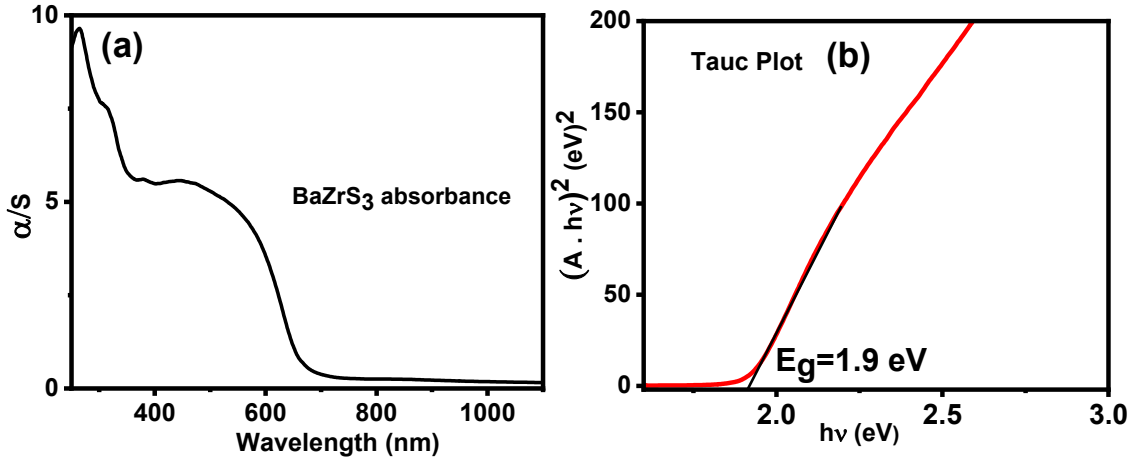

Figure S2: (a) The UV-visible-NIR absorption spectrum is obtained through Kubelka−Munk transformation from the measured diffused reflectance spectra of $BaZrS_3$ NCs powder, where α is the absorption coefficient and S is the scattering coefficient, (b) Tauc plot obtained from the corresponding absorption spectrum showing a direct bandgap of 1.9 eV. After the solid state synthesis, the product was ground, and the fine powder was used to measure absorption spectra. If we measure absorption spectrum of the as synthesized sample before grinding, then the obtained bandgap is around 1.8 eV. The origin of this minor increase in bandgap after grinding is not yet clear.

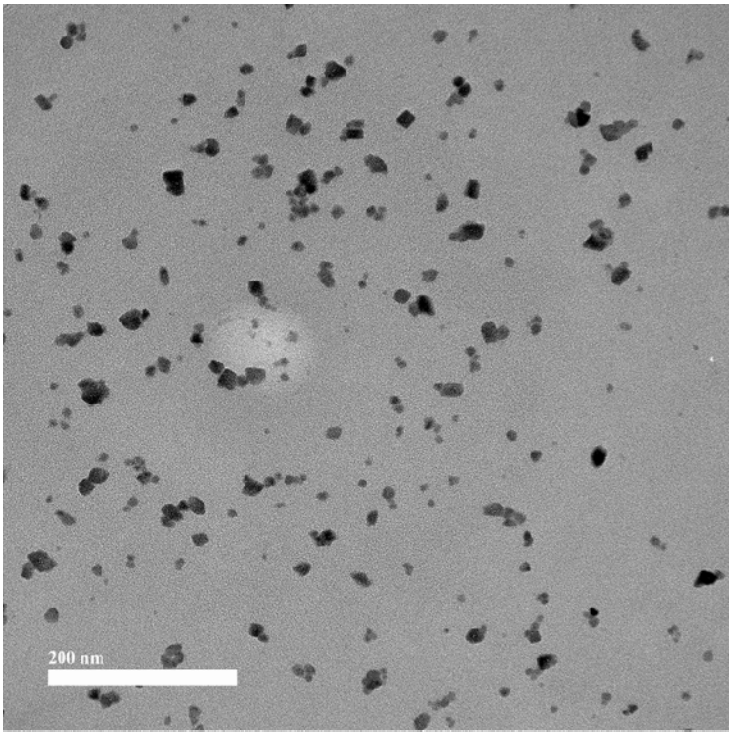

Figure S3: TEM image of $BaZrS_3$ NCs powder prepared by mixing the powder with n-butanol. It shows irregular morphology and particles overlapped on each other.

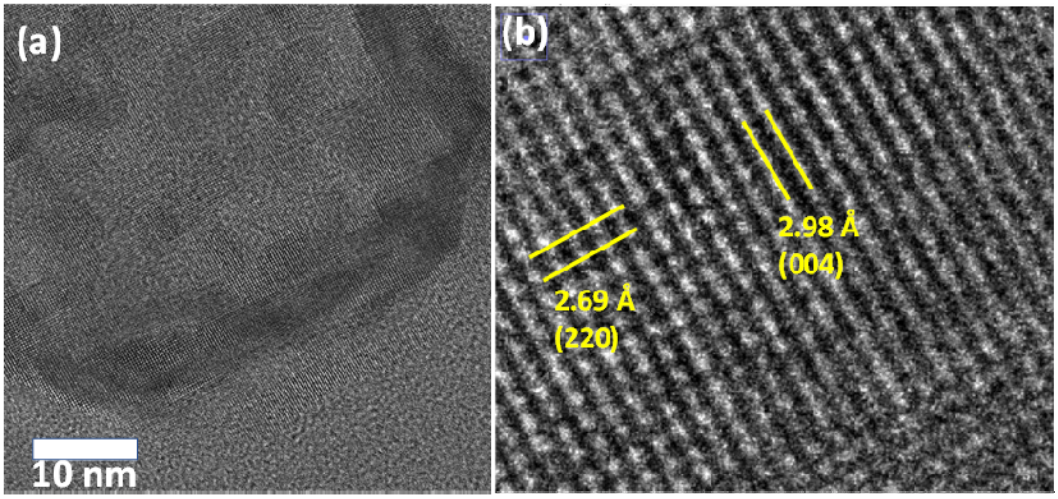

Figure S4: (a) HRTEM image of $BaZrS_3$ NCs powder and (b) magnified image of same to show the lattice fringes. Interplanar distances are marked, 2.98 Å and 2.69 Å corresponding to (004) and (220) planes of orthorhombic $BaZrS_3$ respectively.

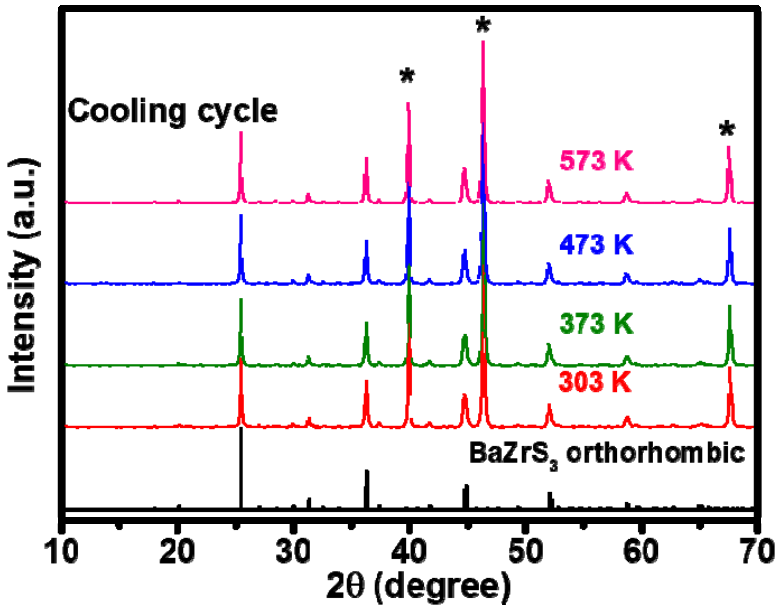

Figure S5: PXRD data of $BaZrS_3$ NCs powder while cooling down the sample from 573 to 303 K. Peaks marked with "*" is due to Pt substrate.

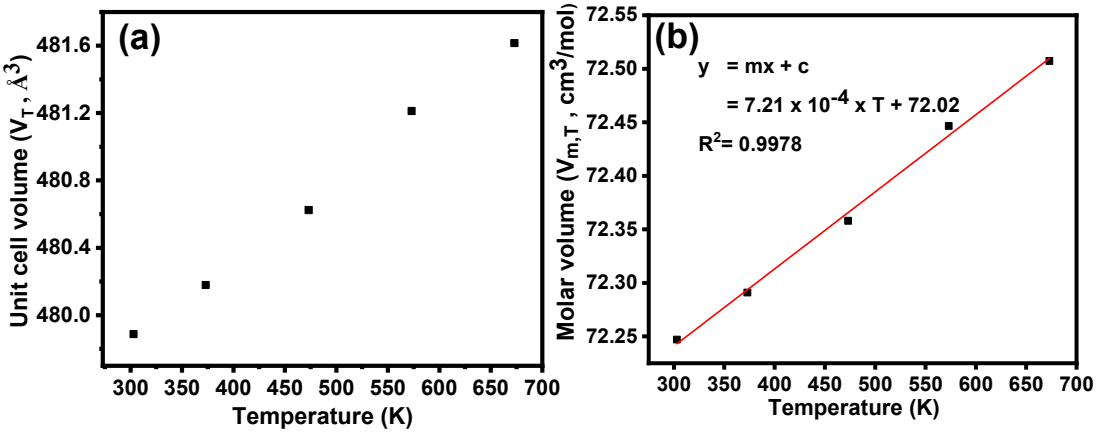

Figure S6: (a) It shows the variation of unit cell volume (V_T) of $BaZrS_3$ with increasing temperature determined using variable temperature PXRD. To obtain this, unit cell constants i.e. a, b and c are determined at each temperature and multiplied to give unit cell volume of orthorhombic crystal structure. (b) It shows the variation of molar volume ($V_{m,T}$) of $BaZrS_3$ with increasing temperature. Molar volume ($V_{m,T}$) are calculated as a function of temperature as $V_{m,T} = V_T \times N_A/Z$,[S12] where V_T is the volume of the unit cell at temperature T, N_A is Avogadro number and Z is the number of formula unit per unit cell (for orthorhombic crystal structure, Z= 4). Coefficient of volume thermal expansion, α_v at temperature T is defined as $\alpha_{v,T} = (1/V_{m,T}) \times (dV_{m,T} / dT)$ (at a constant pressure).[12] In the measured temperature range molar volume can be taken as linear function of temperature and is fitted with the linear equation as shown in inset. The $\alpha_{v,T}$ at 300 K is then determined by dividing the slope (7.21×10^{-4}) with molar volume at 303 K (72.32 cm^3/mol) and is equal to, $\alpha_{v,303\ K} = 9.97\times10^{-6}$ K^{-1}.

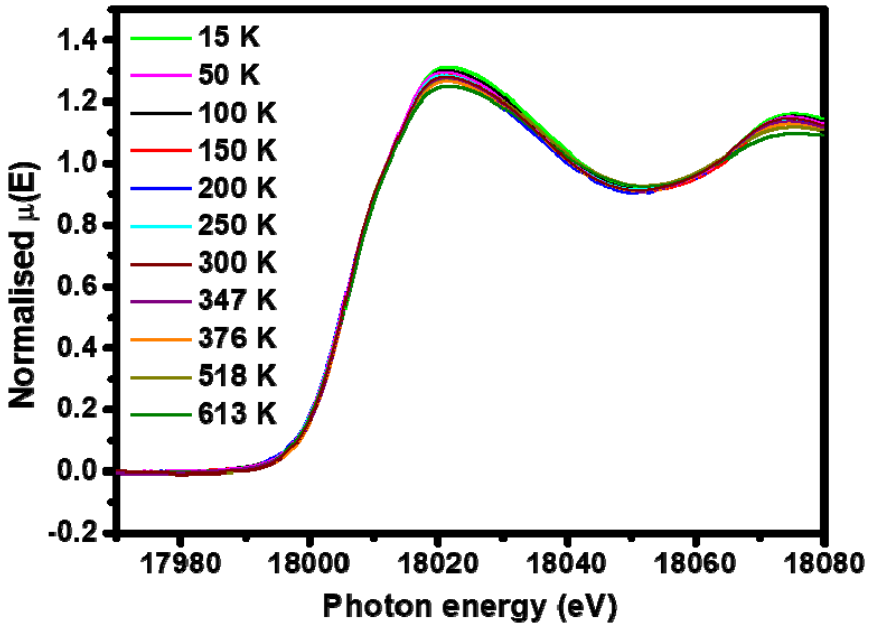

Figure S7: Zr K edge XANES spectra of $BaZrS_3$ NCs at different temperatures.

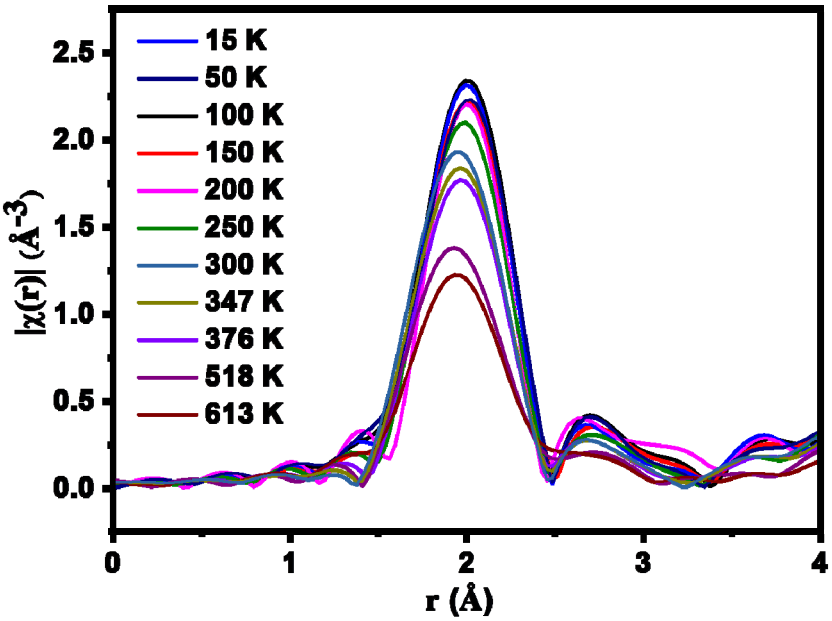

Figure S8: EXAFS data in real space showing $\chi(r)$ versus r plots of the $BaZrS_3$ NCs at different temperatures. A peak near 2 Å is observed. The amplitude of this peak decreases with increase in temperature.

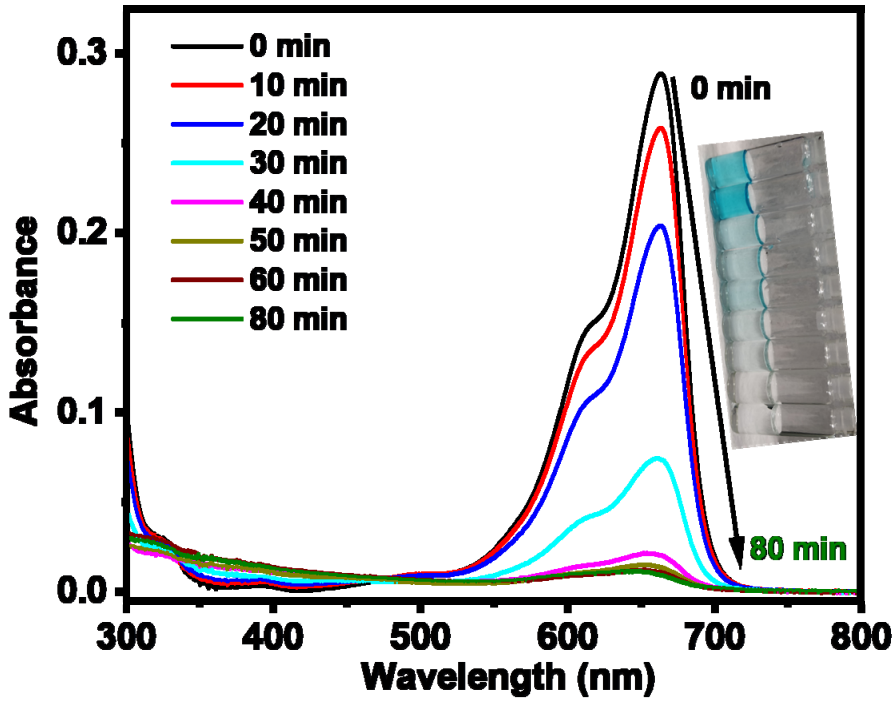

Figure S9: UV-visible absorption spectra of methylene blue dye in water at different irradiation times (using sunlight) in the presence of $BaZrS_3$ NCs. Inset shows digital photographs of methylene blue at different irradiation time.

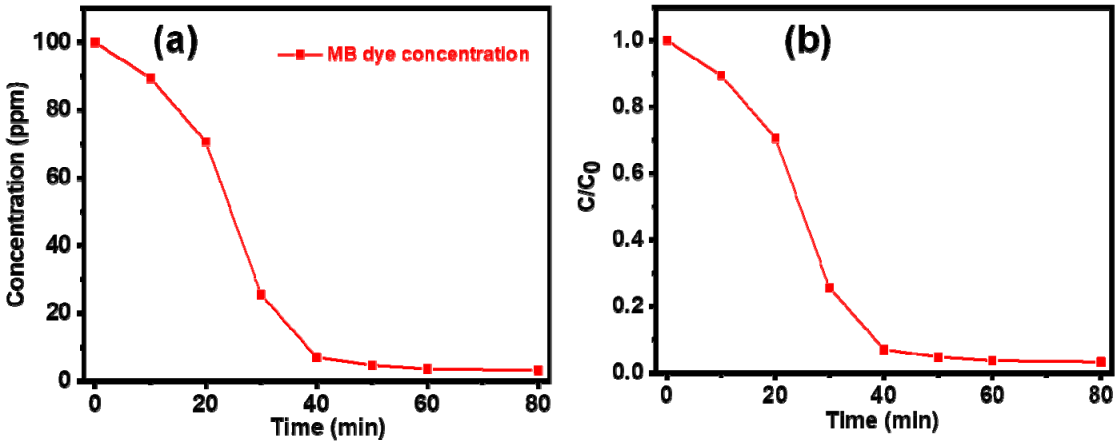

Figure S10: (a) Concentration of methylene blue (MB) dye with increasing time after sunlight irradiation. (b) Plot of C/C_0 versus the irradiation time for the photodegradation of methylene blue dye in presence of $BaZrS_3$ NCs. C_o is concentration of dye at time = 0 min and C is concentration at time = t min. These data are extracted from UV-visible absorption spectra shown in Figure S10.

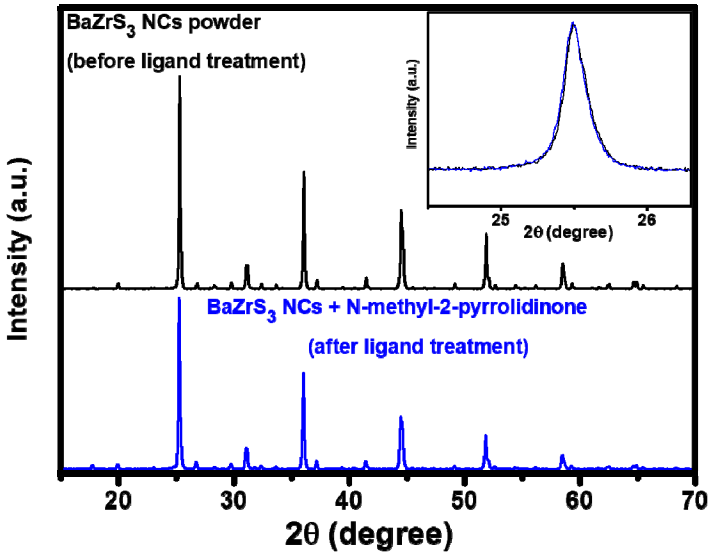

Figure S11: XRD pattern recorded of the film made by drop casting colloidal dispersion of $BaZrS_3$ NCs (treating with N-methyl-2-pyrrolidinone as ligand and heated at 120 °C) compared with the XRD pattern of synthesized $BaZrS_3$ NCs powder. Inset shows that FWHM (full width at half maximum) of XRD peaks remains similar suggesting similarity in size of the $BaZrS_3$ NCs before and after it is heated during the ligand treatment process.

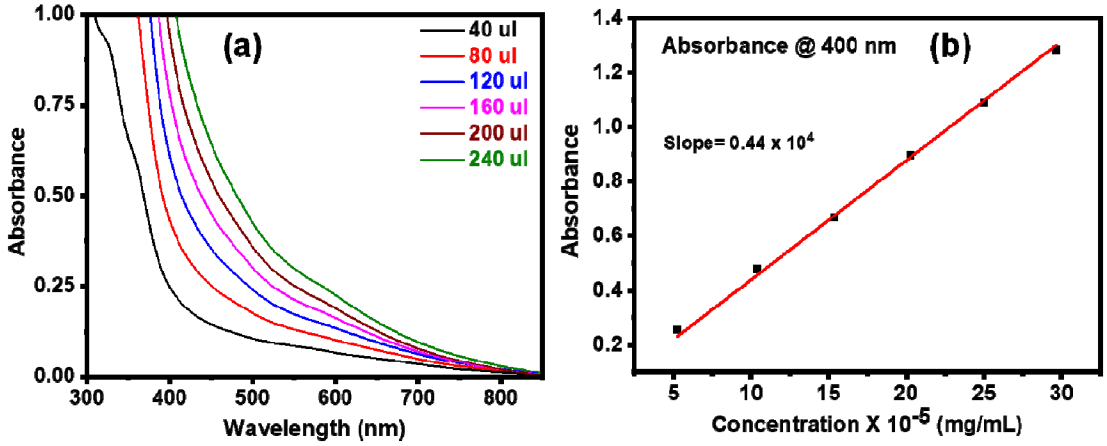

Figure S12: (a) UV-visible spectra of different concentrations of $BaZrS_3$ NCs dispersion in N-methyl-2-pyrrolidinone. (b) Plot of absorbance vs molar concentration (mg/mL) of $BaZrS_3$ NCs obtained by using the spectra in (a).

Field Effect Transistor (FET) device geometry and control experiments:

In the manuscript, we use highly n-doped Si-wafer as a gate electrode and sol-gel processed ZrO_x as a gate dielectric layer. Then the thin film of $BaZrS_3$ NCs is deposited and Au source/drain electrodes are deposited. The schematic device figure is shown below (Figure S13a).

For control measurements, we also fabricated two new types of device geometries: (i) the FET using ZrO_x dielectric without $BaZrS_3$ NCs (Figure S13b and Figure S14), and (ii) the FET with the $BaZrS_3$ NCs deposited on a 300 nm thick SiO_2 dielectric (Figure S13c and Figure S15).

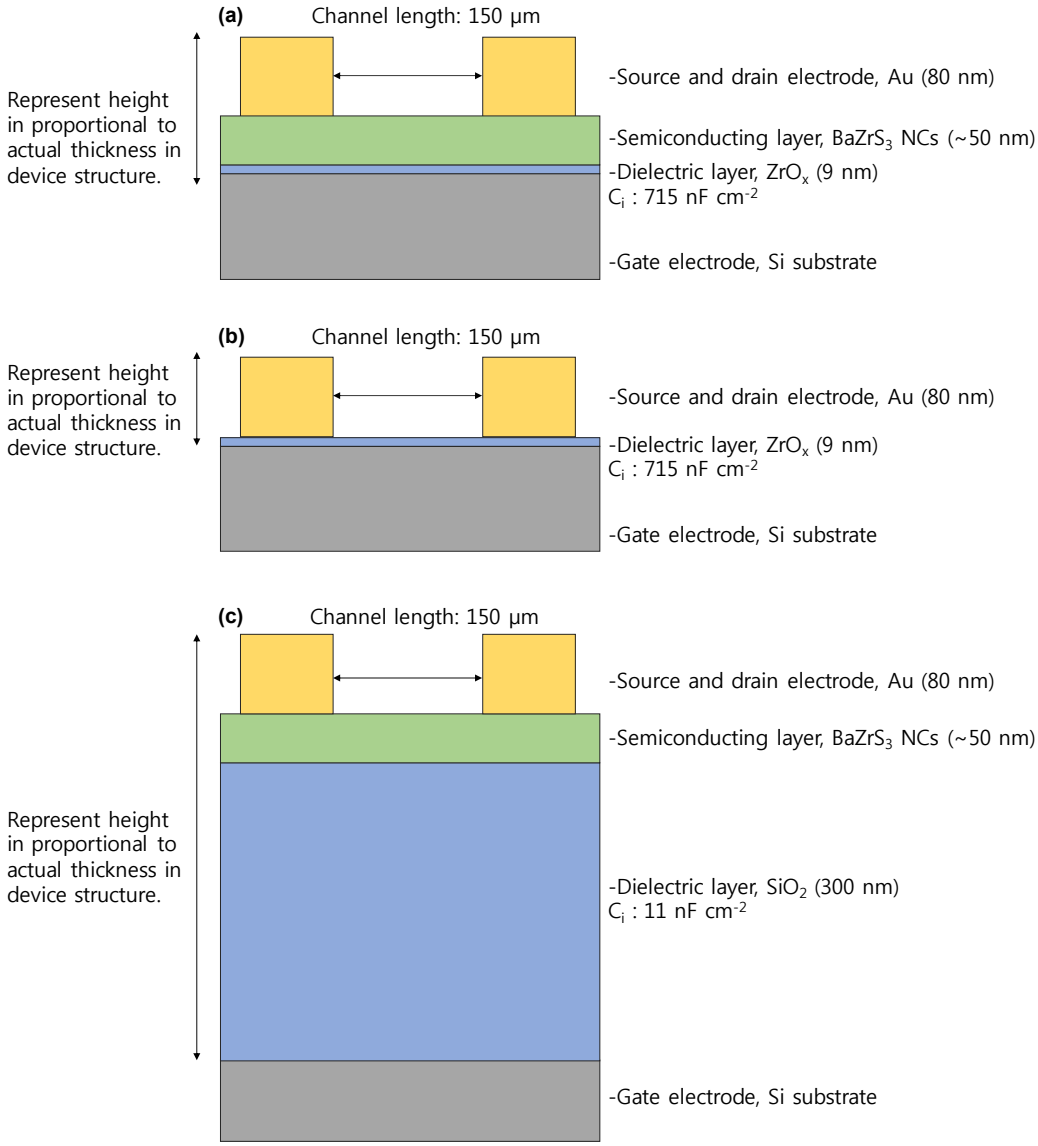

Figure S13: The device geometry of (a) the FET using ZrO_x dielectric (transistor platform in the original manuscript), (b) the FET using ZrO_x dielectric but without $BaZrS_3$ NCs, and (c) the FET using SiO_2 dielectric.

In the case of FET without $BaZrS_3$ NCs layer (Figure S13b), no current modulation as a function of gate bias sweep is observed, as shown in the transfer curves in Figure S14. The ZrO_x layer has a very dense structure and thus even thin ZrO_x layer is sufficient to possess strong dielectric screening properties. These control experiments infer that the FET

characteristics of $BaZrS_3$ NCs shown in the manuscript, do not get influenced by any possible leakage current from the Si gate electrode.

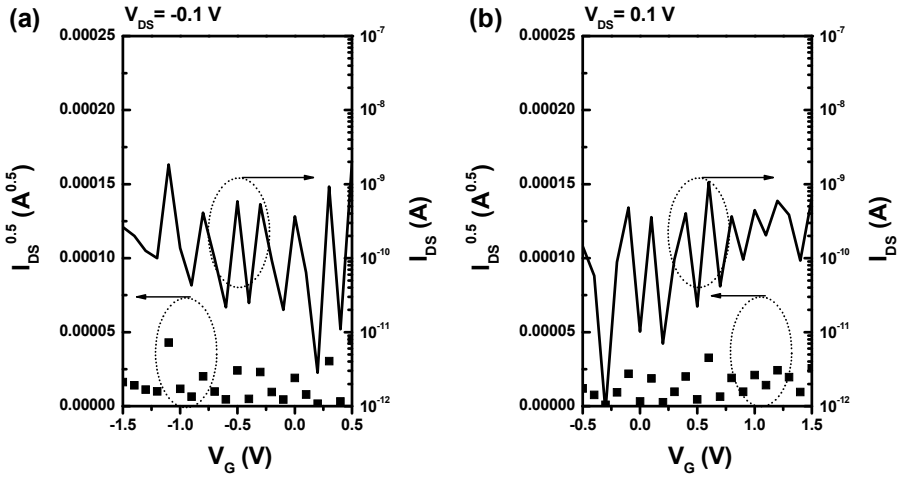

Figure S14: Transfer curves of (a) p-type (V_{DS} = -0.1 V), and (b) n-type (V_{DS} = 0.1 V) in the FET using ZrO_x dielectric without $BaZrS_3$ NCs.

In the case of FET with thick (300 nm) SiO_2 dielectric layer and $BaZrS_3$ NCs layer (Figure S13c), we observe typical ambipolar behavior, similar to the results shown in manuscript (Figure S15). The FETs with SiO_2 layers show lower hole/electron mobilities compared to the ZrO_x FET. This is because the high-k dielectric such as ZrO_x can strongly reduce the impurity scattering compared to low-k dielectric such as SiO_2.[13, 14] This is why we have used ZrO_x dielectric in the manuscript.

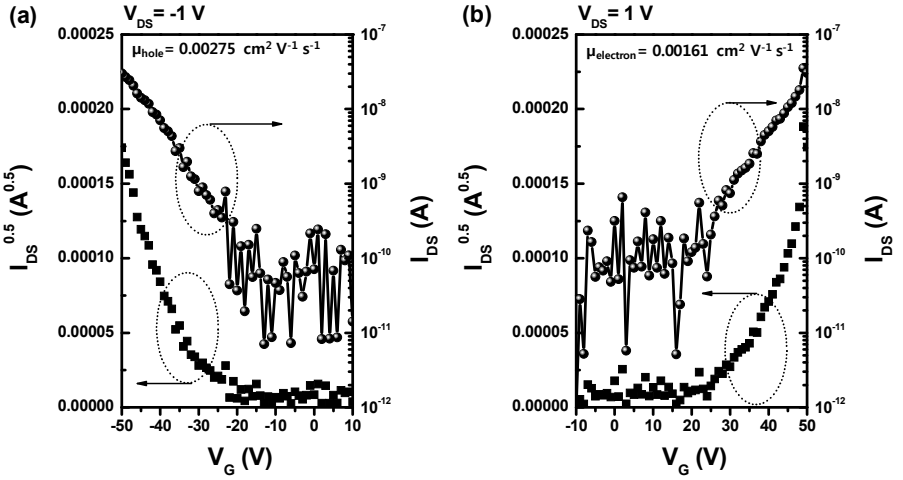

Figure S15: Transfer characteristics of (a) p-type (V_{DS} = -1 V), and (b) n-type (V_{DS} = 1 V) measured condition of pristine film-based devices using SiO_2 (300 nm) dielectric layer.

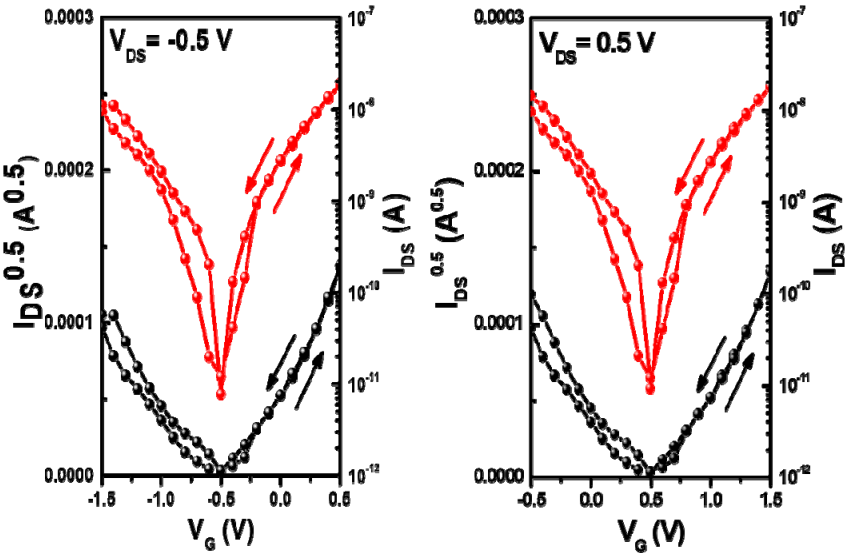

Figure S16: Transfer characteristics of pristine film (prepared at room temperature without annealing) measured in the dual sweep mode, a) p-type, b) n-type measurement conditions.

Table S1: The best fit parameter of $\chi(r)$ versus r EXAFS data shown in Figure S9 and Figure 1e of the manuscript. The experimental data have been fitted from 1-2.5 Å assuming one Zr-S shell at 2.562(6×) Å. The coordination number of this path (N = 6) is kept fixed during the fitting and the bond distances and disorder (Debye-Waller) factors (σ^2), which give the mean-square fluctuations in the distances, have been used as fitting parameters.

Temperature (K)	Zr-S (×6)	
	r (Å)	σ^2 (Å^2)
15	2.529±0.008	0.0043±0.0013
50	2.537±0.011	0.0051±0.0007
100	2.529±0.013	0.0043±0.0009
150	2.531±0.011	0.0045±0.0018
200	2.527±0.016	0.0054±0.0031
250	2.521±0.012	0.0051±0.0021
300	2.527±0.006	0.0055±0.0009
347	2.529±0.005	0.0066±0.0008
376	2.529±0.006	0.0073±0.0009
518	2.501±0.015	0.0098±0.0025
613	2.505±0.014	0.0136±0.0023

Supporting References:

1. S. Niu, H. Huyan, Y. Liu, M. Yeung, K. Ye, L. Blankemeier, T. Orvis, D. Sarkar, D. J. Singh, R. Kapadia and J. Ravichandran, *Adv. Mater.,* 2017, **29,** 1604733.

2. J.-T. Jang, S. Jeong, J.-W. Seo, M. -C. Kim, E. Sim, Y. Oh, S. Nam, B. Park and J. Cheon, *J. Am. Chem. Soc.,* 2011, **133,** 7636-7639.

3. D. M. Balazs, D. N. Dirin, H. -H. Fang, L. Protesescu, G. H. ten Brink, B. J. Kooi, M. V. Kovalenko and M. A. Loi, *ACS Nano*, 2015, **9,** 11951-11959.

4. A. K. Poswal, A. Agrawal, A. K. Yadav, C. Nayak, S. Basu, S. R. Kane, C. K. Garg, D. Bhattachryya, S. N. Jha and N. K. Sahoo, *AIP Conf. Proc.,* 2014, **1591,** 649-651.

5. S. Basu, C. Nayak, A. K. Yadav, A. Agrawal, A. K. Poswal, D. Bhattacharyya, S. N. Jha and N. K. Sahoo, *J. Phys.: Conf. Ser.*, 2014, **493,** 012032.

6. D. C. Konigsberger and R. Prince, X-Ray Absorption: Principles, Applications, Techniques of EXAFS, SEXAFS and XANES. Wiley: New York, 1988.

7. S. Kelly, D. Hesterberg and B. Ravel, Methods of soil analysis. Part 5, 387-463, 2008.

8. G. Bunker, Introduction to XAFS: A Practical Guide to X-ray Absorption Fine Structure Spectroscopy. Cambridge University Press, Cambridge, 2010.

9. M. Newville, B. Ravel, D. Haskel, J. J. Rehr, E. A. Stern and Y. Yacoby, *Physica B.*, 1995, **208-209,** 154-156.

10. Z. Huo, S.-H. Wei and W.-J. Yin, *J. Phys. D: Appl. Phys.,* 2018, ***51,*** 474003.

11. J. W. Bennett, I. Grinberg and A. M. Rappe, *Phys. Rev. B,* 2009, ***79,*** 235115.

12. N. C. Corsepius, T. C. DeVore, B. A. Reisner and D. L. Warnaar, *J. Chem. Educ.,* 2007, **84,** 818-821.

13. A. Konar, T. Fang and D. Jena, *Phys. Rev. B*, 2010, **82,** 115452.

14. X. Liu, Y. Chai and Z. Liu, *Nanotechnol.*, 2017, **28,** 164004.